

2H NMR studies on the dynamics of supercooled water in a metal-organic framework








Verena Schiller, Katharina Knippen, Alois Loidl, Peter Lunkenheimer, Dirk Volkmer, Michael Vogel

Angaben zur Veröffentlichung / Publication details:

Schiller, Verena, Katharina Knippen, Alois Loidl, Peter Lunkenheimer, Dirk Volkmer, and Michael Vogel. 2023. "2H NMR studies on the dynamics of supercooled water in a metal-organic framework." *Journal of Chemical Physics* 159 (3): 034501.
<https://doi.org/10.1063/5.0159256>.

RESEARCH ARTICLE | JULY 17 2023

^2H NMR studies on the dynamics of supercooled water in a metal–organic framework

Verena Schiller ; Katharina Knippen ; Alois Loidl ; Peter Lunkenheimer ; Dirk Volkmer ; Michael Vogel  



J. Chem. Phys. 159, 034501 (2023)


<https://doi.org/10.1063/5.0159256>




View
Online



Export
Citation




Lock-in Amplifier



Boxcar Averager

Boost Your Optics and Photonics Measurements

 Zurich Instruments

[Find out more](#)

^2H NMR studies on the dynamics of supercooled water in a metal–organic framework

Cite as: J. Chem. Phys. 159, 034501 (2023); doi: 10.1063/5.0159256

Submitted: 22 May 2023 • Accepted: 26 June 2023 •

Published Online: 17 July 2023



Verena Schiller,¹ Katharina Knippen,² Alois Loidl,³ Peter Lunkenheimer,³ Dirk Volkmer,² and Michael Vogel^{1,a)}

AFFILIATIONS

¹Institute for Condensed Matter Physics, Technische Universität Darmstadt, Hochschulstraße 6, 64289 Darmstadt, Germany

²Chair of Solid State and Materials Chemistry, Institute of Physics, University of Augsburg, Universitätsstraße 1, 86159 Augsburg, Germany

³Experimental Physics V, Center for Electronic Correlations and Magnetism, University of Augsburg, Universitätsstraße 1, 86159 Augsburg, Germany

^{a)}Author to whom correspondence should be addressed: michael.vogel@pkm.tu-darmstadt.de

ABSTRACT

We use ^2H nuclear magnetic resonance (NMR) to study water (D_2O) reorientation and diffusion in the metal–organic framework MFU-4l, which features a regular three-dimensional network of nearly spherical pores with diameters of 1.2 and 1.9 nm. We observe that the rotational correlation times follow Vogel–Fulcher–Tammann and Arrhenius ($E_a = 0.48$ eV) relations above ~ 225 K and below ~ 170 K, respectively, whereas the temperature dependence continuously evolves from one to the other behavior in the broad crossover zone in between. In the common temperature range, the present NMR results are fully consistent with previous broadband dielectric spectroscopy (BDS) data on water (H_2O) in a very similar framework. Several of our observations, e.g., rotational–translational coupling, indicate that a bulk-like structural (α) relaxation is observed above the crossover region. When cooling through the crossover zone, a quasi-isotropic reorientation mechanism is retained, while ^2H spin-lattice relaxation evolves from exponential to nonexponential, implying that the water dynamics probed at low temperatures does no longer fully restore ergodicity on the time scale of this experiment. We discuss that the latter effect may result from bulk-like and/or confinement-imposed spatially heterogeneous water properties. Comparison with previous NMR and BDS results for water in other confinements reveals that, for confinement sizes around 2 nm, water reorientation depends more on the pore diameter than on the pore chemistry, while water diffusion is strongly affected by the connectivity and topology of the pores.

© 2023 Author(s). All article content, except where otherwise noted, is licensed under a Creative Commons Attribution (CC BY) license (<http://creativecommons.org/licenses/by/4.0/>). <https://doi.org/10.1063/5.0159256>

I. INTRODUCTION

Water, while being the most important liquid on earth, remains a popular topic of ongoing research because a clear understanding of its interesting properties is still lacking. The origin of water's well-known anomalies is supposed to lie in its deeply supercooled temperature regime, which is, however, largely inaccessible because of rapid crystallization, leading to a “no man's land.”¹ Nanoconfinement suppresses the crystallization of water so that cooling the liquid to temperatures below the homogeneous nucleation temperature $T_H = 235$ K becomes possible.^{2–4} Studies on the structure and dynamics of confined water in a broad temperature range are, thus, of high interest in regard to the properties of bulk water and also in itself due to many occurrences of confined water in

nature and technology. Accordingly, the topic has been explored in many scientific studies using different types of confinements and methods.^{5–7}

Commonly, changes in the temperature dependence of water dynamics were found in the supercooled regime, but the locations and interpretations of the observed dynamical crossovers varied considerably. Most studies reported one or even two dynamical crossovers in the temperature range of ~ 160 – 225 K.^{5–8} Several authors described changes in the temperature dependence as a fragile-to-strong transition related to a liquid–liquid phase transition of bulk water.^{9–11} By contrast, others attributed them to an increasing relevance of finite-size effects upon cooling^{12–14} or to a switchover from structural (α) relaxation to a secondary (β) relaxation.^{15–17}

In such studies, it is very important that the entire confined water remains liquid down to a glassy arrest. For example, partial crystallization in confinement can lead to the situation that emergence of the frozen fraction further restricts the volume accessible to the liquid fraction, which, as a result, shows a dynamical crossover from bulk-like to interface-dominated motion.^{18–20} Moreover, a coexistence and interplay of two water fractions interfere with rigorous analysis of experimental data. Therefore, it is crucial to use confinements with well-defined size, which is sufficiently small to entirely avoid crystallization and, when intending to obtain insights into bulk behaviors, at the same time, sufficiently large to perturb water's properties as little as possible. Often, confinement sizes of ~ 2 nm were regarded as a good compromise.^{5–7}

Most of the abovementioned studies on the dynamical crossovers of confined water exploited the fact that mesoporous silica, in particular, MCM-41 materials, have narrow and adjustable pore size distributions. Therefore, it is a pressing question to which degree the observations depend on the chemistry and shape of these confinements. Specifically, MCM-41 features silanol groups, which can be ionized in contact with water, resulting in substantial surface charge, and cylindrical pores with high aspect ratios. A number of studies have addressed the relevance of confinement chemistry by confining water to matrices formed by various types of macromolecules, e.g., proteins,^{21–25} but these approaches suffer from the irregular sizes and shapes of these geometrical restrictions. A few studies used well-defined confinements to systematically investigate the influence of surface chemistry.^{26–28} However, the conclusions on the relevance of this confinement parameter were different.

Several workers have exploited the fact that metal-organic frameworks (MOFs) exhibit well-defined three-dimensional networks of pores with adjustable sizes.^{14,29,30} Some of us used a MOF, which is more hydrophobic than MCM-41 and features regularly arranged and suitably narrow pores. It enables displacements in all spatial directions but still suppresses crystallization of water completely.¹⁴ Employing broadband dielectric spectroscopy (BDS), they observed that the rotational correlation times of the embedded water (H_2O) follow the Vogel-Fulcher-Tammann (VFT) relation above ~ 175 K and the Arrhenius (ARR) relation below. To rationalize their observations, the authors of the work of Fischer *et al.* conjectured that the cooperativity length scale of the α relaxation grows upon cooling and gives rise to the VFT behavior but reaches the confinement size at ~ 175 K so that the degree of cooperativity becomes independent of temperature and a crossover to an ARR behavior occurs.¹⁴

Here, we employ ^2H nuclear magnetic resonance (NMR) to investigate D_2O dynamics in a MOF very similar to that used in the BDS study of Fischer *et al.*¹⁴ Explicitly, we perform ^2H spin-lattice relaxation (SLR), line-shape analysis (LSA), and stimulated-echo (STE) studies to determine the correlation times τ and microscopic mechanisms for water reorientation in a broad temperature range from ambient conditions down to the glass transition. Moreover, we use ^2H static field gradient (SFG) diffusometry to measure self-diffusion coefficients D . Such a combination of ^2H NMR methods proved to be very suitable to study the molecular dynamics of various liquids in nanoscale confinements.^{26,31–36} Thus, the present NMR approach provides comprehensive insights into rotational and translational D_2O dynamics in MOF confinement and, in this way, complements the previous BDS study.¹⁴ To

determine the relevance of the chemistry and shape of confinements for the behavior of water, we compare the results for the MOF host with those of our previous ^2H NMR and BDS studies using MCM-41 pores of comparable sizes.^{8,18,19,31–33}

II. SAMPLES AND METHODS

Preparation and characterization of the used MOF^{14,37} and measurement and analysis of ^2H NMR data for confined D_2O ^{18,19,31,32} have been previously described in some detail. Therefore, we restrict ourselves to a short overview in the following text.

A. Sample preparation and characterization

We use a MOF host, which is similar to that employed in the work of Fischer *et al.*¹⁴ There, MFU-4l-HCOO was utilized, where the acronym “MFU” means Metal Organic Framework Ulm University, “l” stands for “large,” and “HCOO” indicates that the Cl^- ligands, which provide charge compensation and point inside the pores, were substituted for HCOO^- ones. Here, we utilize the original material with the Cl^- ligands to avoid proton-deuteron exchange between the framework and water. Details about the preparation of the host material can be found in previous studies.^{14,37} We refer to the employed framework as MFU-4l in the following text. A schematic representation of water-loaded MFU-4l is shown in Fig. 1. MFU-4l features two types of nearly spherical pores with diameters of 1.2 and 1.9 nm, which form a regular three-dimensional network.³⁷ The specific pore volume amounts to $1.3 \text{ cm}^3/\text{g}$, as determined from argon adsorption at 77 K.³⁷ Calorimetric measurements ruled out a crystallization of significant fractions of water inside the MFU-4l.¹⁴

To load the MFU-4l powder with D_2O , we followed a protocol previously established in our studies on water in mesoporous silica.³⁸ First, the host material was filled into NMR tubes and dried in high

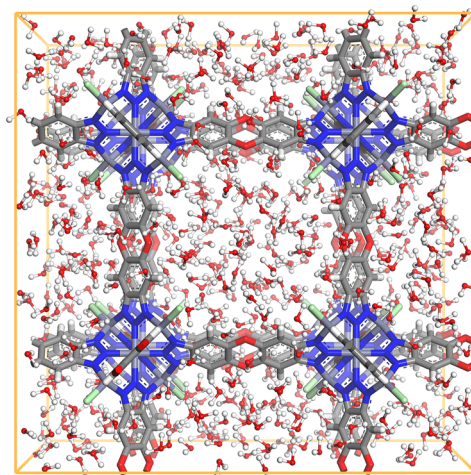


FIG. 1. Stick model of the used MFU-4l host material, illustrating the three-dimensional pore network. The pores are filled with water molecules to depict the situation in the studied sample.

vacuum ($p < 10^{-5}$ mbar) for at least 24 h. Afterward, a micropipette was used to add an appropriate amount of D_2O as calculated based on the mass of the dried framework material and the specific pore volume. The used amount corresponds to a pore filling factor of 90%, which ensures the absence of excess water, as confirmed by the following 2H NMR results. Finally, the NMR tubes were flame-sealed and stored for several days before starting the measurements to ensure thermal equilibrium.

B. 2H NMR methodology

In 2H SFG studies, a magnetic field with a static gradient g is applied so that the 2H Larmor frequencies ω_L depend on the nuclear positions and, hence, their fluctuations provide access to the self-diffusion coefficient D .^{39,40} We use the STE pulse sequence to correlate the Larmor frequencies during two evolution times t_e , which are separated by a variable mixing time t_m . In this case, the observed STE decays depend on the diffusivity D according to^{39,40}

$$S(t_m) \propto \exp \left[-Dq^2 \left(t_m + \frac{2}{3}t_e \right) \right]. \quad (1)$$

Here, it is assumed that, unlike the cylindrical MCM-41 pores,³³ the MFU-4l host does not lead to deviations from three-dimensional diffusion. Moreover, $q = \gamma g t_e$ can be considered as a generalized scattering vector, where γ is the gyromagnetic ratio of the deuterons. The inverse q^{-1} determines the length scale of the diffusion measurement. We exploit that our SFG setup provides access to strong field gradients $g > 100$ T/m and use evolution times up to $t_e = 300 \mu s$ to achieve q^{-1} below $1 \mu m$, which is smaller than the MFU-4l particle size of $3-4 \mu m$.³⁷ Therefore, our 2H SFG STE measurements probe D_2O diffusion within the MFU-4l framework largely unperturbed by grain boundary effects. In the supplementary material, this is confirmed by the observation that the diffusion coefficients D are independent of the value of t_e and, thus, of the experimental length scale $q^{-1} \propto t_e^{-1}$ when using sufficiently long evolution times $t_e > 150 \mu s$.

In a homogeneous magnetic field B_0 , our 2H NMR experiments probe the quadrupolar frequencies ω_Q of the deuterons, which depend on the orientations of the D_2O molecules, explicitly, on the angles θ between the B_0 field and the O–D bond,

$$\omega_Q = \pm \frac{\delta}{2} (3 \cos^2 \theta - 1) \propto P_2(\cos \theta), \quad (2)$$

where $\delta = 2\pi \cdot 161$ kHz describes the strength of the quadrupolar interaction.¹⁸ Because the quadrupolar frequencies ω_Q are proportional to the second Legendre polynomial $P_2(\cos \theta)$, their fluctuations provide access to the rotational correlation function $F_2(t)$ of the D_2O molecules.

In 2H SLR experiments, we fit the buildup of the 2H magnetization $M(t)$ after saturation with a modified Kohlrausch–Williams–Watts (KWW) function given by

$$M(t) = M_0 \left[1 - \exp \left(- \left(\frac{t}{T_1} \right)^{\beta_{SLR}} \right) \right], \quad (3)$$

where M_0 denotes the equilibrium magnetization, T_1 is the spin-lattice relaxation time, and β_{SLR} is the stretching parameter. T_1

is related to the rotational motion of the D_2O molecules by the Bloembergen–Purcell–Pound (BPP) equation⁴¹

$$\frac{1}{T_1(\omega_L)} = \frac{2}{15} \delta^2 [J_2(\omega_L) + 4J_2(2\omega_L)]. \quad (4)$$

Here, $J_2(\omega)$ denotes the spectral density associated with the correlation function $F_2(t)$. $T_1(T)$ exhibits a minimum when water reorientation obeys $\omega_L \tau = 0.616$, yielding a correlation time of ~ 1 ns at this temperature in our case. To determine correlation times at other temperatures, knowledge about the shape of $J_2(\omega)$ is required but not necessarily available in the first place.

We obtain information about the shape of the spectral density from field-cycling relaxometry (FCR), which allows one to measure T_1 over a broad range of Larmor frequencies using a rapidly switchable electromagnet.^{42–44} In our 2H FCR approach, the T_1 dispersion provides straightforward access to the spectral density J_2 based on Eq. (4).^{45,46} For further analysis, it proved to be useful to multiply the measured SLR rates $1/T_1(\omega_L)$ with the respective Larmor frequencies ω_L to move from a spectral density to a dynamical susceptibility representation,^{8,45,46}

$$\begin{aligned} \frac{\omega_L}{T_1(\omega_L)} &= \frac{2}{15} \delta^2 [\omega_L J_2(\omega_L) + 4\omega_L J_2(2\omega_L)] \\ &= \frac{2}{15} \delta^2 [\chi_2''(\omega_L) + 2\chi_2''(2\omega_L)] \equiv \chi_{NMR}''(\omega_L). \end{aligned} \quad (5)$$

Motivated by our 2H FCR results, we assume a Havriliak–Negami (HN) susceptibility⁴⁷ in the present 2H SLR analysis,

$$\chi_{HN}(\omega) = \chi_\infty + \frac{\chi_0 - \chi_\infty}{[1 + (i\omega\tau_{HN})^{\alpha_{HN}}]^{\beta_{HN}}}. \quad (6)$$

It involves the time constant τ_{HN} , the shape parameters α_{HN} and β_{HN} , and the low-frequency and high-frequency limits, χ_0 and χ_∞ , respectively. Furthermore, for straightforward comparison with BDS results, we calculate peak correlation times τ_p from the fit parameters,⁴⁸

$$\frac{\tau_p}{\tau_{HN}} = \left[\sin \left(\frac{\pi \alpha_{HN} \beta_{HN}}{2(\beta_{HN} + 1)} \right) \right]^{\frac{1}{\alpha_{HN}}} \left[\sin \left(\frac{\pi \alpha_{HN}}{2(\beta_{HN} + 1)} \right) \right]^{-\frac{1}{\alpha_{HN}}}. \quad (7)$$

2H LSA studies provide access to rotational motions in the microseconds regime. In the limit of slow reorientation ($\tau \gg \delta^{-1}$), the orientation dependence of ω_Q leads to a broad 2H NMR spectrum termed Pake spectrum for powder samples. In the limit of fast reorientation ($\tau \ll \delta^{-1}$), motionally narrowed 2H NMR spectra are observed. Their shape depends on the motional mechanism, e.g., a narrow Lorentzian line results from liquid-like isotropic reorientation. The transition from broad low-temperature to narrow high-temperature line shapes is accompanied by a minimum of the signal intensity in the solid-echo sequence used to record the spectra. Specifically, a solid-echo intensity minimum indicates a correlation time of $\tau \approx \delta^{-1} \approx 1 \mu s$.²³

For slow dynamics with correlation times in the milliseconds range, 2H STE studies in homogenous magnetic fields enable a direct measurement of rotational correlation functions.^{49,50} Here,

we correlate the quadrupolar frequencies ω_Q and, thus, the D_2O orientations before and after the mixing time t_m according to

$$F_2^{cc}(t_m) \propto \langle \cos[\omega_Q(0)t_e] \cos[\omega_Q(t_m)t_e] \rangle. \quad (8)$$

Considering that, in addition to D_2O reorientation, T_1 relaxation contributes to the STE decays, we fit the experimental data with

$$F_2^{cc}(t_m) \propto \left[(1 - F_\infty) \exp \left[- \left(\frac{t_m}{\tau_K} \right)^{\beta_K} \right] + F_\infty \right] R_{SLR}. \quad (9)$$

In doing so, we describe the decay due to D_2O reorientation by a modified KWW function, which is characterized by the correlation time τ_K and stretching parameter β_K and includes a residual correlation F_∞ to account, e.g., for the possibilities of an immobile water fraction or an anisotropy of water reorientation. Moreover, we exploit that the SLR damping R_{SLR} can be determined in independent SLR measurements and fixed in the STE fits. Peak correlation times τ_p are available from the fit parameters τ_K and β_K according to²⁶

$$\frac{\tau_p}{\tau_K} = 1.785 - 0.871\beta_K - 0.029\beta_K^2 + 0.114\beta_K^3. \quad (10)$$

C. Experimental setups

The 2H SLR, LSA, and STE studies were performed using two homebuilt spectrometers, which operate at a 2H Larmor frequency of $\omega_L = 2\pi \cdot 46$ MHz. Additional SLR measurements were carried out at $\omega_L = 2\pi \cdot 25$ MHz. The SLR and LSA approaches employed solid-echo readout sequences with a solid-echo delay of 20 μs . The STE measurements utilized a four-pulse sequence with appropriate phase cycling to overcome the dead time of the receiver and to avoid unwanted single and double quantum coherences.⁵¹ For 2H SFG diffusometry, we employed a custom-made magnet featuring a pair of superconducting coils in anti-Helmholtz arrangement to produce very strong magnetic field gradients.⁴⁰ The sample was placed at a position characterized by a 2H Larmor frequency of $\omega_L = 2\pi \cdot 25$ MHz and a magnetic field gradient of $g = 140$ T/m. In all these 2H NMR measurements, the 90° pulse length was between 2.0 and 2.5 μs , ensuring appropriate excitation of the broad 2H frequency dispersions. The FCR setup and methodology was thoroughly described in previous studies.^{43,52} It features an electromagnet with a field switching time of ~ 1 ms, which sets the lower limit for the accessible T_1 times. In all setups, the temperature accuracy was better than ± 1 K and the temperature stability better than ± 0.5 K. Further details about the NMR equipment and methods can be found elsewhere.^{31,33,53,54}

III. RESULTS

A. Self-diffusion coefficients

First, we use 2H SFG NMR to investigate translational dynamics of D_2O in MFU-4l. In the supplementary material, 2H SFG STE decays $S(t_m)$ for various evolution times t_e and temperatures T are presented together with fits based on Eq. (1). In Fig. 2, we show the resulting self-diffusion coefficients D , which are limited to $T \geq 255$ K due to the interference of 2H SLR at lower temperatures. In the accessible range, the temperature dependence of the self-diffusion

FIG. 2. Self-diffusion coefficients D from 2H SFG measurements on D_2O in MFU-4l together with an Arrhenius fit, which yields an activation energy of $E_a = 0.37$ eV. Our results are compared with previous 1H and 2H SFG data for bulk D_2O ,⁵⁵ which are described by an activation energy of $E_a = 0.22$ eV, and for H_2O (squares) and D_2O (circles) in MCM-41 pores with the indicated diameters.³³

coefficients can be described by an ARR law with an activation energy of $E_a = 0.37$ eV, but we anticipate based on the previous BDS¹⁴ and following NMR results that non-ARR behavior develops at sufficiently low temperatures. A comparison with previous results⁵⁵ for bulk D_2O reveals that the MFU-4l confinement leads to a slowdown of the diffusion by a factor of five at 290 K and to an increase in activation energy by a factor of almost two. Moreover, it is evident from Fig. 2 that the diffusion coefficients D in the MFU-4l host do not agree with those in MCM-41 pores with a similar size of ~ 2 nm but rather with those in MCM-41 pores with a larger diameter of 2.8 nm,³³ where the discrepancies between H_2O and D_2O are mild, while the activation energy E_a is similar in all these confinements. The respective analyses in the present and previous³³ SFG approaches remove trivial differences arising from the fact that water diffusion involves a different number of spatial dimensions in the MFU-4l framework and MCM-41 pores. Therefore, the finding that, for a given confinement size, diffusion is faster in MFU-4l than in MCM-41 may result from different water–host interactions and/or from diverse confinement shapes and connectivities. We will continue this discussion after our studies of water reorientation.

B. Spin-lattice relaxation

To characterize the rotational motion of D_2O in MFU-4l, we first analyze 2H SLR. In Fig. 3, we see from exemplary data that the magnetization $M(t)$ builds up in a single step at the studied temperatures (135–290 K). This implies that any discrepancy in the dynamical behaviors of deuterons is moderate and, hence, there are no deuterons other than those of liquid water; particularly, there is no evidence for ice or framework deuterons. The absence of an ice fraction shows that water outside the pores, which would freeze, does not exist and that water inside the pores does not crystallize in the covered temperature range. The absence of a contribution from the framework confirms that our approach exclusively probes the water. Thus, the monomodal 2H SLR of the MFU-4l sample makes the interpretation of data simpler than in previous approaches using silica confinements,^{18–20,31,32} where $M(t)$ usually showed a bimodal buildup at sufficiently low temperatures. Still, 2H SLR of D_2O in MFU-4l becomes nonexponential upon cooling and, hence, KWW fits are required for an appropriate analysis; see Eq. (3).

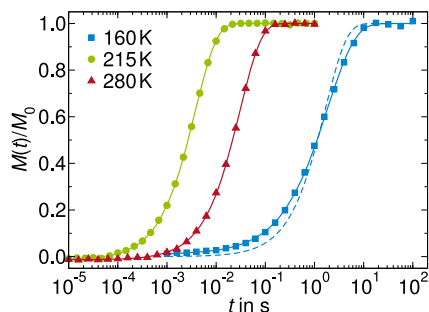


FIG. 3. Buildup of normalized magnetization $M(t)/M_0$ for three exemplary temperatures at a ^2H Larmor frequency of $\omega_L = 2\pi \cdot 46$ MHz. The solid lines are fits with Eq. (3), yielding stretching parameters of $\beta_{\text{SLR}} = 1$ at both higher temperatures and $\beta_{\text{SLR}} = 0.76$ at 160 K. To illustrate the nonexponentiality of the buildup at 160 K, an exponential fit (dashed line) is shown for comparison.

Figure 4 shows the SLR times T_1 and stretching parameters β_{SLR} obtained from the KWW fits of $M(t)$ at various temperatures and for Larmor frequencies ω_L of $2\pi \cdot 25$ and $2\pi \cdot 46$ MHz. We observe a T_1 minimum at 221 and 228 K for the lower and higher frequencies, respectively. Such a shift is expected because faster dynamics at higher temperatures is required to meet the minimum criterion $\omega_L \tau = 0.616$ for higher frequencies ω_L . The T_1 values at the minima are larger than expected for a Debye process, indicating that water reorientation exhibits a distribution of correlation times. For both Larmor frequencies, ^2H SLR is exponential ($\beta_{\text{SLR}} = 1$) down to 200 K and becomes increasingly nonexponential upon cooling below this temperature until the stretching parameter levels off at $\beta_{\text{SLR}} \approx 0.8$ near 165 K. As was discussed in more detail in previous ^2H SLR studies on confined D_2O ,^{31,32} these findings imply that, above 200 K, the water molecules exchange their correlation times on the milliseconds to seconds scales of the magnetization buildup, e.g., by exploring different spatial regions within the framework, while this exchange is too slow to fully average the dynamical heterogeneities on the T_1 time scale at lower temperatures. Analogous ^2H SLR studies^{18,20,25,31,32} on D_2O in mesoporous silica and protein matrices reported T_1 and β_{SLR} results, which agree with the present ones qualitatively but not quantitatively. In Fig. 4, exemplary results¹⁸ for an MCM-41 confinement are included, revealing also the bimodal nature of ^2H SLR in those samples. Generally, the ^2H T_1 times are shorter for confined D_2O than for bulk D_2O near ambient temperatures, indicating that the host materials cause a slowdown of water reorientation, as will be quantified below.

To determine temperature-dependent correlation times from T_1 data, knowledge about the frequency dependence of the spectral density J_2 is required. Previous approaches to confined water assumed, e.g., Cole–Davidson (CD) or Cole–Cole (CC) shapes, but unambiguous information was often lacking, resulting in substantial uncertainties at temperatures well above or below the T_1 minimum.^{23,25} Therefore, we exploit that FCR provides insight into $J_2(\omega_L)$.^{44–46} Very recently, this approach was successfully applied to determine the shape of the spectral density associated with reorientation dynamics of confined liquids, including water.^{8,46} To avoid framework contributions, we do not use the more common ^1H FCR,

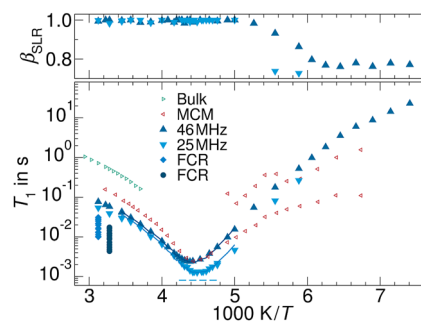


FIG. 4. ^2H SLR time T_1 and stretching parameter β_{SLR} at Larmor frequencies ω_L of $2\pi \cdot 25$ and $2\pi \cdot 46$ MHz. The dashed horizontal line indicates the minimum value of T_1 calculated for a Debye process, i.e., a Lorentzian spectral density, and $\omega_L = 2\pi \cdot 25$ MHz. The solid lines are T_1 times back calculated for the respective Larmor frequencies using a HN spectral density characterized by $\alpha_{\text{HN}} = 0.75$, $\beta_{\text{HN}} = 0.815$, and the correlation times $\tau_{\text{HN}}(T)$ from our ^2H SLR analyses; see Fig. 8. For comparison, results for D_2O in the bulk (see the supplementary material) and in MCM-41 with a pore diameter of 2.1 nm¹⁸ are included ($\omega_L = 2\pi \cdot 46$ MHz). In the MCM-41 confinement, ^2H SLR was bimodal below 210 K. At 305 and 320 K, ^2H FCR is used to measure T_1 in a broader frequency range. The observed frequency dependence $T_1(\omega_L)$ is shown in Fig. 5.

but rather apply ^2H FCR. For D_2O in MFU-4L, ^2H FCR is only applicable at sufficiently high frequencies and temperatures because the method is not capable of probing the short ^2H T_1 times in the minimum region and the nonexponential ^2H SLR hampers the analysis at low temperatures. Specifically, we measure ^2H T_1 for Larmor frequencies ω_L between 2.6×10^5 and 2.9×10^7 s⁻¹ at 305 and 320 K. Figure 5 displays the obtained SLR rates $1/T_1(\omega_L)$ and the NMR susceptibilities $\chi''_{\text{NMR}}(\omega_L)$ calculated therefrom. While T_1 does not depend on ω_L for bulk D_2O at these temperatures well above the T_1 minima, it shows significant frequency dependence for confined D_2O . Due to the limited frequency and temperature ranges, we do not observe the $\chi''_{\text{NMR}}(\omega_L)$ peak associated with water reorientation but merely its low-frequency flank. As expected based on the T_1 dispersion, we find for D_2O in MFU-4L that the low-frequency flank of the susceptibility peak does not show the ω_L^{-1} behavior of the bulk liquid, but its frequency dependence is described by a power law $\omega_L^{-0.75}$ at both temperatures. Similarly, power-law exponents smaller than unity were reported in ^2H FCR studies on water and ethylene glycol in MCM-41.^{8,46} Thus, the slope of the low-frequency flank indicates clear deviations from bulk-like CD behavior so that it is not appropriate to employ the CD spectral density in the present ^2H SLR analysis. A CC spectral density would allow for a low-frequency dispersion, but using our knowledge from the FCR study and setting its width parameter to 0.75 does not reproduce the observed heights of the T_1 minima.

Considering these results, we assume a HN spectral density with a temperature-independent shape for the ^2H SLR analysis. In this case, it is possible to exploit the knowledge from our ^2H FCR studies to fix $\alpha_{\text{HN}} = 0.75$, ensuring the correct low-frequency slope, and to determine β_{HN} from the height of the T_1 minimum. The analysis yields $\beta_{\text{HN}} = 0.85$ at $2\pi \cdot 25$ MHz and $\beta_{\text{HN}} = 0.78$ at $2\pi \cdot 46$ MHz. Using the thus determined HN spectral densities in Eq. (4), τ_{HN} is obtained from T_1 . Based on these results for the HN time constants and shape parameters, we calculate the peak correlation times

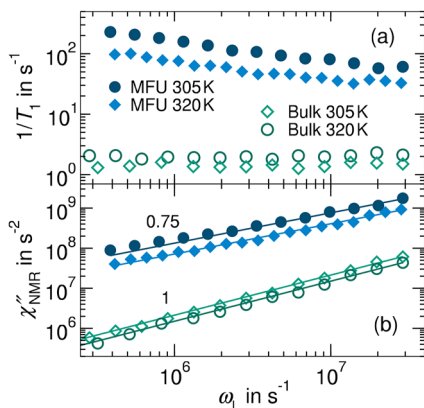


FIG. 5. Results from ^2H FCR on D_2O in the bulk and the MFU-4l confinement: (a) Dependence of the SLR rate $1/T_1$ on the Larmor frequency ω_L and (b) NMR susceptibilities $\chi''_{\text{NMR}}(\omega_L)$ obtained therefrom. The lines are interpolations with power laws ω_L^1 and $\omega_L^{0.75}$ for bulk and confined D_2O , respectively.

τ_p according to Eq. (7). They will be shown below together with the correlation times from the following LSA and STE studies. For a consistency check, we use the HN spectral density characterized by $\alpha_{\text{HN}} = 0.75$ and the average $\beta_{\text{HN}} = 0.815$ of the observed values together with the obtained time constants $\tau_{\text{HN}}(T)$ to back calculate the $T_1(T)$ curves for the used Larmor frequencies ω_L of $2\pi \cdot 25$ and $2\pi \cdot 46$ MHz. Reinspection of Fig. 4 confirms that our approach well describes the temperature and frequency dependence of T_1 .

Altogether, the present ^2H SLR analysis yields a HN susceptibility with low-frequency and high-frequency flanks of $\alpha_{\text{HN}} = 0.75$ and $-\alpha_{\text{HN}}\beta_{\text{HN}} = -0.61$, respectively. Thus, the HN susceptibility from our NMR study has a weakly asymmetric shape, which mildly differs from the symmetric CC susceptibility from the BDS approach.¹⁴ Considering that a crossover from asymmetric to symmetric susceptibility shape occurred when cooling water in silica pores,⁸ this mild difference may well result from the fact that the shape of the NMR and BDS susceptibilities was determined at different temperatures. Specifically, the SLR analysis involved high temperatures above and near the T_1 minima, whereas the BDS analysis was affected from an overlap of other processes in this range and, thus, was mainly based on low-temperature data. In passing, we note that, unlike in ^1H FCR, a low-frequency broadening does not result from intermolecular relaxation contributions in ^2H FCR.^{45,46} This difference results from the facts that the dipolar interaction, which involves not only intramolecular but also intermolecular contributions, dominates for ^1H , whereas the quadrupolar interaction, which is of single-particle nature, governs our ^2H results.

C. Line-shape analysis

In Fig. 6, we display the ^2H NMR spectra of D_2O in MFU-4l at various temperatures. We see a transition from a broad Pake spectrum to a narrow Lorentzian line between ~ 190 and 200 K, indicating that D_2O reorientation dynamics crosses the microsecond time scale of LSA upon heating. This line-shape transition is accompanied by a minimum in the solid-echo intensity at 196 K (see the supplementary material), which reveals a correlation time of

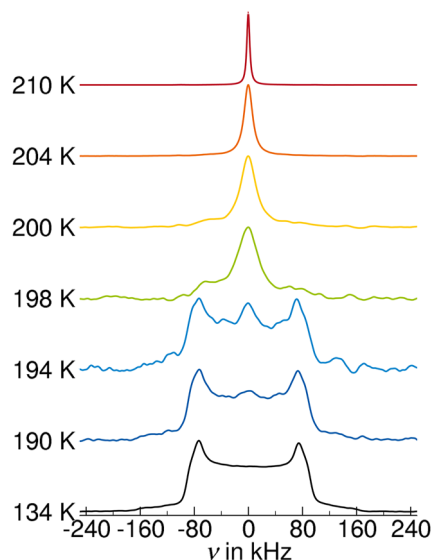


FIG. 6. ^2H NMR spectra of D_2O in MFU-4l at the indicated temperatures.

$\sim 1 \mu\text{s}$.²³ During the transition, the spectra can roughly be described as a weighted superposition of Pake and Lorentz components. This implies a coexistence of D_2O molecules, which are slow and fast with respect to $\tau = \delta^{-1}$, and, thus, confirms the heterogeneous nature of water reorientation. The two-component line shape occurs in a temperature interval of ~ 10 K for D_2O in MFU-4l, indicating that the distribution of correlation times has a moderate width. For comparison, this line shape was observed over significantly broader temperature intervals for D_2O in other confinements, explicitly, between 180 and 210 K in MCM-41 pores¹⁸ and even between 170 and 230 K in an elastin matrix,²⁵ whereas the distribution of correlation times is often too narrow to produce two-component spectra for the α process of bulk supercooled liquids, e.g., glycerol.⁵⁶ As for the motional mechanism, the observed Lorentzian line shape indicates that D_2O reorientation is quasi-isotropic down to at least ~ 200 K in MFU-4l.

D. Stimulated-echo experiments

Finally, we perform ^2H STE studies on D_2O in MFU-4l to investigate slow rotational motion at low temperatures. The resulting correlation functions $F_2^{\text{cc}}(t_m)$ are shown in Fig. 7. The decays are nonexponential and shift to longer times upon cooling, reflecting the heterogeneity and slowdown of D_2O reorientation, until they become governed by additional SLR damping near 145 K. For a quantitative analysis, we fit the STE decays with Eq. (9), which combines a modified KWW function to describe D_2O reorientation with a predetermined SLR damping function. The peak correlation times τ_p calculated from the KWW fit parameters according to Eq. (10) will be compared with previous BDS results¹⁴ in the following discussion. The obtained stretching parameters amount to $\beta_K \approx 0.35$, indicating substantial nonexponentiality of the correlation functions. Similar stretching parameters were reported for D_2O in MCM-41,³¹ while the nonexponentiality was even higher for

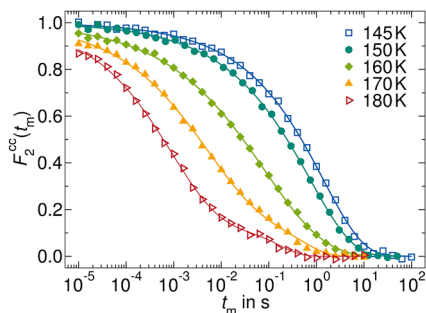


FIG. 7. Correlation function $F_2^{cc}(t_m)$ for D_2O in MFU-4l at various temperatures, as obtained from 2H STE measurements for evolution times of $t_e \approx 6 \mu s$. The lines are fits with Eq. (9). The measured STE decays were normalized to $F_2^{cc}(0) = 1$ based on the fit results. The data for 145 and 180 K are shown as open symbols to indicate that parts of these correlation decays occur outside the experimental time window, $t_e < t_m < T_1$, interfering with a reliable determination of the residual correlation F_∞ and leading to larger uncertainties of the extracted correlation times at these temperatures.

D_2O in an elastin matrix ($\beta_K \approx 0.27$)²³ and somewhat lower for bulk supercooled liquids ($\beta_K \approx 0.4$ – 0.5).^{57–59} Furthermore, the fits yield small residual correlations, which decrease from $F_\infty = 0.15$ to $F_\infty = 0.03$ when decreasing the temperature in the studied range. This means that D_2O dynamics causes a nearly complete loss of orientational correlation and, hence, the motion remains quasi-isotropic even at temperatures as low as ~ 150 K. We note that molecular dynamics during the evolution times t_e of the experiment usually leads to an artificial enhancement of the residual correlation F_∞ in $F_2^{cc}(t_m)$ measurements.^{60–62} We expect that this experimental artifact causes the higher residual correlations $F_\infty = 0.15$ observed at higher temperatures of the studied range, where the correlation loss partly occurs at $t_m < 10 \mu s$ and, thus, water dynamics during the used evolution times $t_e \approx 6 \mu s$ is no longer negligible. Therefore, the true values should amount to $F_\infty < 0.1$ in the whole temperature range, further corroborating the quasi-isotropic nature of D_2O reorientation dynamics in MFU-4l.

IV. DISCUSSION

Combining the information from our 2H SFG, SLR, LSA, and STE analyses, we are able to follow D_2O dynamics in MFU-4l confinement over a broad temperature range. In Fig. 8, we compare the correlation times from our studies with results for bulk and confined water from previous approaches. All data indicate a highly nontrivial temperature dependence of water dynamics.

First, we focus on the high-temperature range of our SFG, SLR, and LSA approaches to D_2O in MFU-4l. It can be seen in Fig. 8 that the SLR peak correlation times τ_p obtained for different Larmor frequencies coincide. Furthermore, they are in harmony with the LSA result at a slightly lower temperature. At ambient conditions, MFU-4l confinement causes a slowdown of D_2O reorientation by a factor of 2–3, depending on temperature, as can be seen by comparison with correlation times from an additional 2H SLR analysis for a D_2O bulk sample (see the supplementary material). At ~ 225 K, the temperature dependence of τ_p shows a mild crossover. Above the crossover, it can be described by the VFT relation, $\tau_p = \tau_\infty$

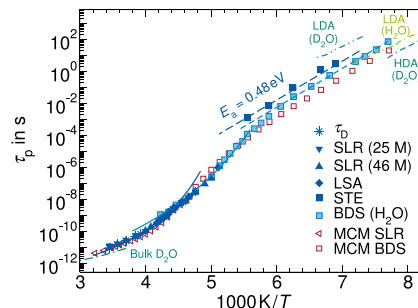


FIG. 8. Correlation times of D_2O (dark blue) and H_2O (light blue) in MFU-4l: Peak correlation times τ_p of D_2O and H_2O from the present 2H SLR, LSA, and STE studies and previous BDS work,¹⁴ respectively, together with “diffusion correlation times” τ_D from 2H SFG diffusometry. The SLR results involve Larmor frequencies ω_L of $2\pi \cdot 25$ and $2\pi \cdot 46$ MHz. The τ_D data were calculated from the diffusion coefficients D using the SED relation and a hydrodynamics radius of $R_H = 1.2 \text{ nm}$. The solid lines are (extrapolated) VFT fits of the SLR data above 225 K ($\tau_\infty = 2.1 \cdot 10^{-14} \text{ s}$, $B = 753 \text{ K}$, $T_0 = 163 \text{ K}$) and of the BDS data above 175 K ($\tau_\infty = 6.2 \cdot 10^{-15} \text{ s}$, $B = 1379 \text{ K}$, $T_0 = 122 \text{ K}$).¹⁴ The dashed lines are ARR laws with an activation energy of $E_a = 0.48 \text{ eV}$. For comparison, previous SLR and BDS results for D_2O in MCM-41 pores with a diameter of 2.1 nm (red symbols)⁸ and for bulk H_2O (light green line) and bulk D_2O (dark green lines) are included. The high-temperature bulk results were determined in our additional 2H SLR studies on bulk D_2O and correspond to mean rather than peak correlation times, but one expects that both values differ only mildly (see the supplementary material). The low-temperature bulk data were obtained in BDS work from heating low-density (LDA) and equilibrated high-density (HDA) amorphous ices through their glass transitions.⁶⁴

$\exp[B/(T - T_0)]$, with $B = 753 \text{ K}$ and $T_0 = 163 \text{ K}$. Below the crossover, the SLR results agree with previous BDS data for H_2O in a similar MFU-4l host, which followed a VFT relation with $B = 1379 \text{ K}$ and $T_0 = 122 \text{ K}$.¹⁴ In the supplementary material, we show that a description of the SLR results with a single VFT function is not adequate.

A comparison with SLR and BDS findings⁸ for D_2O in MCM-41 reveals minor differences. Explicitly, in MCM-41, the dynamical crossover occurred at a somewhat lower temperature of $\sim 215 \text{ K}$ and it was more prominent. Differences regarding the position and degree of the crossover result from the fact that the curvature of the temperature-dependent τ_p values in the Arrhenius plot is weaker in MFU-4l than in MCM-41 above the crossover, whereas the temperature dependence is similar in both confinements not too far below. For H_2O in MCM-41, a quasi-elastic neutron scattering study reported a mild crossover at 225 K for a pressure of 1 bar, which shifted to 219 K when increasing the pressure to 4 kbar.⁶³ Thus, the exact position and degree of this crossover at $\sim 225 \text{ K}$ depend on the confinement conditions. Below, we will return to the question whether a bulk or a confinement effect is the expected underlying reason for the existence of this phenomenon.

In the narrow temperature range of our 2H SFG study, 255–290 K, it is possible to compare the translational and rotational motions of D_2O in MFU-4l. For this purpose, we use the Stokes–Einstein–Debye (SED) relation given by

$$D\tau_D = \frac{2}{9} R_H^2 \quad (11)$$

to calculate “diffusion correlation times” τ_D from the measured self-diffusion coefficients D . In doing so, the hydrodynamics radius is set to $R_H = 1.2 \text{ \AA}$, which allows for best possible overlap with the peak correlation times τ_p . In Fig. 8, we observe that translational and rotational D_2O dynamics have a very similar temperature dependence in the range available for this comparison. This agreement together with the VFT temperature dependence, which is clearly seen only at lower temperatures, imply that our 2H NMR approaches probe the α relaxation of D_2O in MFU-4l at least down to the dynamical crossover at $\sim 225 \text{ K}$.

We move on to the low-temperature range of the STE studies. In Fig. 8, we see that the peak correlation times from our STE approach to D_2O and from previous BDS work¹⁴ on H_2O are described by ARR laws with the same activation energy of $E_a = 0.48 \text{ eV}$, but the former are a factor of ~ 3 longer than the latter. Similar activation energies were reported for water in various types of confinements,^{6,7,21} including MCM-41,^{8,32} and when heating high-density amorphous (HDA) or low-density amorphous (LDA) ice phases above their glass transition temperatures T_g .⁶⁴ Despite the common activation energy, the exact values of correlation times differ between various samples. The discrepancies, including the observed difference between the STE data for D_2O and the BDS data for H_2O in MFU-4l, result in large parts from isotope effects. For example, the low-temperature dynamics of H_2O and D_2O also differed by a factor of ~ 3 in MCM-41, irrespective of the used method.^{19,32} Interestingly, larger isotope effects were observed for bulk samples below the no man’s land.^{64,65} Specifically, the correlation times are a factor of ~ 30 longer for amorphous D_2O bulk ice phases than for their H_2O counterparts (see Fig. 8). To avoid isotope effects, we focus on samples containing D_2O for further comparisons. We find that the rotational dynamics of D_2O is about an order of magnitude slower in MFU-4l than in MCM-41 at low temperatures. By contrast, we observed faster translational diffusion for D_2O in the former than the latter confinement at high temperatures (see Fig. 2). Compared to bulk data, the peak correlation times of D_2O in MFU-4l lie roughly midway between those of heated HDA and LDA D_2O phases.

When considering the peak correlation times in the whole temperature range, a crossover between VFT and ARR behaviors is clearly evident. However, it is difficult to pinpoint an exact crossover temperature. Rather, the changes extend from $\sim 225 \text{ K}$, where deviations from the high-temperature VFT relation set in, to $\sim 170 \text{ K}$, where evolution toward the low-temperature ARR law is complete, as is best seen from the previous BDS data.¹⁴ Moreover, the exact temperatures depend on the confinement conditions, as was discussed above, and the hydration level, as observed in previous work.⁶⁶ Despite these minor quantitative differences, the crossover zone is consistently observed in NMR and BDS, for H_2O and D_2O , and in MFU-4l and MCM-41. Together with the reasonable agreement between confined and bulk water dynamics both above and below the no man’s land, these findings imply that the crossover is an intrinsic property of water. Notwithstanding, the exact values and the temperature dependence of the correlation times and, thus, the degree and width of the crossover are affected by specific liquid–matrix interactions and finite-size effects imposed by the respective confinements.

Near the lower end of the crossover zone, 2H SLR becomes nonexponential upon cooling (see Fig. 4). As aforementioned, this

finding means that an exchange between regions with different correlation times becomes too slow to average the dynamical heterogeneity on the time scale of the 2H magnetization buildup. In bulk supercooled liquids, this effect usually occurs when the structural renewal associated with the α relaxation becomes slow with respect to T_1 slightly above T_g .⁶⁷ Here, the nonexponentiality of 2H SLR sets in near 195 K (see Fig. 4), where τ_p amounts to $\sim 10^{-6} \text{ s}$ and, hence, the correlation times are much shorter than $T_1 \approx 10^{-2} \text{ s}$, even if we allow for some distribution of the former. On the other hand, an extrapolation of the high-temperature VFT behavior suggests a correlation time of $\sim 10^{-2} \text{ s}$ at 195 K , which is on the order of T_1 . Therefore, we may not exclude that, although unobserved otherwise, the high-temperature VFT/ α process continues to lower temperatures at least for a water fraction. Taken together, these findings suggest that, despite its quasi-isotropic mechanism, the relaxation process observed in the NMR and BDS studies during and below the crossover region does not fully restore ergodicity and, hence, it differs in this respect from the α process of bulk liquids. Considering that the correlation times of this motion resemble those of heated HDA and LDA ices, one may wonder whether the latter phases exhibit typical bulk-like α dynamics. This leaves the possibilities that the present low-temperature NMR and BDS process is a confinement-specific α relaxation, which does not incorporate all confinement regions alike because of strong internal mobility gradients, or that it is an unusual and water-specific secondary relaxation, which involves quasi-isotropic rotational dynamics and possibly to some extent translational motion but still does not result in an extensive exploration of the MFU-4l framework. In such situations, the high-temperature VFT/ α process could survive and restore ergodicity at lower temperatures for at least a water fraction but would remain unobserved because this water fraction is small or the orientational correlation is largely destroyed by the faster quasi-isotropic secondary relaxation.

The above analyses showed that water dynamics in MFU-4l and MCM-41 confinements are overall similar. Nonetheless, some differences pertaining to the values of the correlation times and diffusion coefficients provide information about the relevance of various confinement effects. Explicitly, the rotational correlation times were slightly and noticeably longer in MFU-4l than in MCM-41 above and below the crossover region, respectively (see Fig. 8). These results provide evidence against a dominant role of the chemical nature of the pore walls in these cases because the interactions of water with the matrix are weaker and, thus, the dynamics of water should be faster in the less hydrophilic MFU-4l than the more hydrophilic MCM-41 if this was the decisive factor. Rather, the slower water reorientation in MFU-4l than MCM-41 implies that the confinement size has a noticeable effect because the former host features narrower pores ($1.2/1.9 \text{ nm}$)³⁷ than the latter (2.1 nm).³² Stronger confinement can lead to an acceleration or slowdown of molecular dynamics, depending on the pore sizes, host materials, and interaction of the confined molecules with the pore walls.^{68,69} An acceleration is usually ascribed to a reduced cooperativity length scale of the molecular motions in confinement.^{70,71} On the other hand, simulation studies^{72–74} revealed that, even if favorable guest–host interactions are absent, liquid dynamics is often strongly retarded near a solid interface so that the observed slower water dynamics in the narrower pores of MFU-4l may well be due to the reduced average distance of the molecules to the pore walls as

compared to the situation in MCM-41. In a previous BDS study,¹⁴ slower water dynamics in MFU-4l than in MCM-41 was reported. There, it was speculated to be due to effectively stronger water confinement in MCM-41, which, despite the nominally larger pore size, could arise from partial water crystallization and/or a layer of immobile molecules close to the pore walls. Thus, the exact reason for the somewhat different water relaxation times in both confinements, revealed by Fig. 8, is not finally clarified yet.

While the local reorientation of water is slower in MFU-4l than in MCM-41, the translational diffusion is faster in the former than the latter host, at least when comparing results for similar confinement sizes near ambient temperatures. This discrepancy means that the short-range dynamics and, hence, the chemistry and size of the individual pores, do not fully control the long-range dynamics, but the connectivity and topology of the pores play an important role for the transport. Specifically, we propose that the open three-dimensional MFU-4l framework imposes weaker obstacles to water diffusion than the separate cylindrical, i.e., quasi-one-dimensional MCM-41 pores, where host imperfections may lead to pore restrictions, which act as diffusion barriers.

V. CONCLUSION

We performed NMR experiments to investigate water dynamics in MFU-4l confinement. While a previous BDS study¹⁴ on a similar sample enabled a more complete analysis of longer correlation times at lower temperatures, showing, e.g., a change in the temperature dependence at ~165–175 K, our NMR approach significantly extended the accessible ranges to faster dynamics and higher temperatures and, in this way, revealed another change in water dynamics near 225 K. Furthermore, ²H NMR unraveled information about motional mechanisms, which is not available from BDS. Therefore, the present NMR and previous BDS studies nicely complement each other. In the temperature range 195–225 K, our ²H NMR findings for D₂O agree with the previous BDS results¹⁴ for H₂O, indicating that isotope effects are negligible for the observed motion. At lower temperatures, D₂O reorients somewhat slower than H₂O, but the isotope effects are substantially smaller than those reported for amorphous bulk water samples.⁶⁴

All ²H NMR results show that D₂O in MFU-4l exhibits notably heterogeneous dynamics, but no bimodal dynamics, which could result from a significantly less mobile interfacial layer or the bimodal pore size distribution of the framework.³⁷ In a high-temperature region above ~225 K, we observed a coupling of rotational and translational dynamics, a VFT temperature dependence, and exponential ²H SLR. Based on these findings, we conclude that the α relaxation of the confined liquid is probed in this range. In a low-temperature region below roughly 170 K, NMR and BDS¹⁴ showed that water reorientation follows an ARR law with an activation energy of $E_a = 0.48$ eV, which is in harmony with previous findings for water in a large variety of confinements.^{5–7} In this range, D₂O reorientation is still quasi-isotropic but ²H SLR is nonexponential, implying that the probed dynamical process does no longer fully restore ergodicity and, hence, deviates in an important aspect from the α relaxation of supercooled bulk liquids. In the broad crossover zone between 170 and 225 K, the temperature dependence of water dynamics continuously evolves from the high-temperature to the low-temperature limits.

Comparisons with literature results^{8,32,33} showed that water dynamics in less hydrophilic MFU-4l and more hydrophilic MCM-41 confinements are similar but not identical. While the overall similarity suggested that the observed temperature dependence reflects at least to some extent intrinsic water behavior, some quantitative differences provided valuable information about the relevance of various confinement effects. Specifically, a discussion of water's correlation times and diffusion coefficients against the backdrop of the MFU-4l and MCM-41 characteristics implied that, in the studied range of confinement parameters, water reorientation depends less on the pore chemistry than on the pore size. Furthermore, our results revealed that diffusive water dynamics are not fully determined by local water dynamics and, hence, by the properties of the individual pores, but are significantly affected by the connectivity and topology of the pores. Altogether, as compared to the situation in MCM-41, the narrower MFU-4l pores are more restrictive for water reorientation, but their three-dimensional arrangement is more favorable for water diffusion. Therefore, we conclude that water dynamics on different length and time scales are governed by different host parameters.

The hypothesis that our findings for confined water reflect intrinsic properties of bulk water is supported by the reasonable agreement of confined and bulk water dynamics above and below the no man's land. However, several observations imply that the dynamical behavior is very complex. Several scientists,^{12–14} including some of us, proposed that a dynamical crossover results when the growing cooperativity length of the α relaxation reaches the confinement size. Although we found evidence for a relevance of geometrical restrictions on water dynamics, the existence of two changes in the temperature dependence and a broad crossover zone together with the observation of a limited capacity of the probed low-temperature motion to restore ergodicity imply that further effects are relevant. In particular, prominent structural and dynamical heterogeneities may be important. If existent, it is unclear whether an inhomogeneous scenario is imposed by confinements or inherent to water. In confinements, heterogeneities can result from different behaviors near the pore walls and in the pore centers. However, even in the bulk, regions with HDL-like and LDL-like structural motifs may form when approaching the proposed second critical point or nanoscopic domains with crystalline order but high concentrations of defects may emerge within the viscous liquid. When such confinement-imposed or bulk-like structural and dynamical heterogeneities exist, the slower component would constitute an intrinsic confinement for the faster one, resembling the situation in dynamically asymmetric mixtures and leading to an altered temperature dependence. Thus, in addition to more common explanations, like altered α relaxation or emerging β relaxation, more subtle phenomena may cause the complex dynamical scenario of cooled water specimen and clever experimental strategies are required to distinguish between these possibilities more accurately in future work.

SUPPLEMENTARY MATERIAL

See the supplementary material for additional ²H NMR diffusion studies, the temperature dependence of the solid-echo intensity, a spin-lattice relaxation analysis for bulk D₂O, and an alternative fit of temperature-dependent NMR correlation times.

AUTHOR DECLARATIONS

Conflict of Interest

The authors have no conflicts to disclose.

Author Contributions

Verena Schiller: Data curation (equal); Formal analysis (equal); Investigation (lead); Methodology (equal); Writing – original draft (equal); Writing – review & editing (supporting). **Katharina Knippen:** Investigation (equal); Methodology (supporting); Resources (supporting); Writing – review & editing (supporting). **Alois Loidl:** Conceptualization (equal); Methodology (supporting); Validation (supporting); Writing – review & editing (equal). **Peter Lunkenheimer:** Conceptualization (equal); Methodology (supporting); Validation (supporting); Writing – review & editing (equal). **Dirk Volkmer:** Conceptualization (equal); Methodology (equal); Resources (equal); Supervision (equal); Writing – original draft (supporting); Writing – review & editing (equal). **Michael Vogel:** Conceptualization (lead); Data curation (supporting); Formal analysis (equal); Investigation (supporting); Methodology (equal); Project administration (lead); Resources (lead); Supervision (lead); Validation (lead); Writing – original draft (equal); Writing – review & editing (lead).

DATA AVAILABILITY

The data that support the findings of this study are available from the corresponding author upon reasonable request.

REFERENCES

- O. Mishima and H. E. Stanley, “The relationship between liquid, supercooled and glassy water,” *Nature* **396**, 329–335 (1998).
- S. Jähnert, F. Vaca Chávez, G. E. Schaumann, A. Schreiber, M. Schönhoff, and G. H. Findenegg, “Melting and freezing of water in cylindrical nanopores,” *Phys. Chem. Chem. Phys.* **10**, 6039–6051 (2008).
- J. Deschamps, F. Audonnet, N. Brodie-Linder, M. Schoeffel, and C. Alba-Simionesco, “A thermodynamic limit of the melting/freezing processes of water under strongly hydrophobic nanoscopic confinement,” *Phys. Chem. Chem. Phys.* **12**, 1440–1443 (2010).
- S. Kittaka, S. Takahara, H. Matsumoto, Y. Wada, T. J. Satoh, and T. Yamaguchi, “Low temperature phase properties of water confined in mesoporous silica MCM-41: Thermodynamic and neutron scattering study,” *J. Chem. Phys.* **138**, 204714 (2013).
- S. Capaccioli, K. L. Ngai, S. Ancherbak, P. A. Rolla, and N. Shinyashiki, “The role of primitive relaxation in the dynamics of aqueous mixtures, nano-confined water and hydrated proteins,” *J. Non-Cryst. Solids* **357**, 641–654 (2011).
- J. Swenson and S. Cerveny, “Dynamics of deeply supercooled interfacial water,” *J. Phys.: Condens. Matter* **27**, 033102 (2015).
- S. Cerveny, F. Mallamace, J. Swenson, M. Vogel, and L. Xu, “Confined water as model of supercooled water,” *Chem. Rev.* **116**, 7608–7625 (2016).
- E. Steinrücken, M. Weigler, V. Schiller, and M. Vogel, “Dynamical susceptibilities of confined water from room temperature to the glass transition,” *J. Phys. Chem. Lett.* **14**, 4104–4112 (2023).
- L. Liu, S.-H. Chen, A. Faraone, C.-W. Yen, and C.-Y. Mou, “Pressure dependence of fragile-to-strong transition and a possible second critical point in supercooled confined water,” *Phys. Rev. Lett.* **95**, 117802 (2005).
- A. Faraone, L. Liu, C.-Y. Mou, C.-W. Yen, and S.-H. Chen, “Fragile-to-strong liquid transition in deeply supercooled confined water,” *J. Chem. Phys.* **121**, 10843–10846 (2004).
- F. Mallamace, M. Broccio, C. Corsaro, A. Faraone, U. Wanderlingh, L. Liu, C.-Y. Mou, and S. H. Chen, “The fragile-to-strong dynamic crossover transition in confined water: Nuclear magnetic resonance results,” *J. Chem. Phys.* **124**, 161102 (2006).
- S. Cerveny, J. Colmenero, and A. Alegria, “Comment on ‘Pressure dependence of fragile-to-strong transition and a possible second critical point in supercooled confined water,’” *Phys. Rev. Lett.* **97**, 189802 (2006).
- S. Cerveny, F. Barroso-Bujans, Á. Alegria, and J. Colmenero, “Dynamics of water intercalated in graphite oxide,” *J. Phys. Chem. C* **114**, 2604–2612 (2010).
- J. K. H. Fischer, P. Sippel, D. Denysenko, P. Lunkenheimer, D. Volkmer, and A. Loidl, “Supercooled water confined in a metal-organic framework,” *Commun. Phys.* **3**, 95 (2020).
- J. Swenson, H. Jansson, and R. Bergman, “Relaxation processes in supercooled confined water and implications for protein dynamics,” *Phys. Rev. Lett.* **96**, 247802 (2006).
- S. A. Lusceac, M. Rosenstihl, M. Vogel, C. Gainaru, A. Fillmer, and R. Böhmer, “NMR and dielectric studies of hydrated collagen and elastin: Evidence for a delocalized secondary relaxation,” *J. Non-Cryst. Solids* **357**, 655–663 (2011).
- S. Capaccioli, K. Ngai, S. Ancherbak, M. Bertoldo, G. Ciampalini, M. S. Thayyil, and L.-M. Wang, “The JG β -relaxation in water and impact on the dynamics of aqueous mixtures and hydrated biomolecules,” *J. Chem. Phys.* **151**, 034504 (2019).
- M. Sattig and M. Vogel, “Dynamic crossovers and stepwise solidification of confined water: A ^2H NMR study,” *J. Phys. Chem. Lett.* **5**, 174–178 (2013).
- C. Lederle, M. Sattig, and M. Vogel, “Effects of partial crystallization on the dynamics of water in mesoporous silica,” *J. Phys. Chem. C* **122**, 15427–15434 (2018).
- Y. Yao, V. Fella, W. Huang, K. A. I. Zhang, K. Landfester, H.-J. Butt, M. Vogel, and G. Floudas, “Crystallization and dynamics of water confined in model mesoporous silica particles: Two ice nuclei and two fractions of water,” *Langmuir* **35**, 5890–5901 (2019).
- S. Cerveny, G. A. Schwartz, R. Bergman, and J. Swenson, “Glass transition and relaxation processes in supercooled water,” *Phys. Rev. Lett.* **93**, 245702 (2004).
- S. Pawlus, S. Khodadadi, and A. P. Sokolov, “Conductivity in hydrated proteins: No signs of the fragile-to-strong crossover,” *Phys. Rev. Lett.* **100**, 108103 (2008).
- M. Vogel, “Origins of apparent fragile-to-strong transitions of protein hydration waters,” *Phys. Rev. Lett.* **101**, 225701 (2008).
- W. Doster, S. Busch, A. M. Gaspar, M. S. Appavou, J. Wuttke, and H. Scheer, “Dynamical transition of protein-hydration water,” *Phys. Rev. Lett.* **104**, 098101 (2010).
- S. A. Lusceac, M. R. Vogel, and C. R. Herbers, “ ^2H and ^{13}C NMR studies on the temperature-dependent water and protein dynamics in hydrated elastin, myoglobin and collagen,” *Biochim. Biophys. Acta, Proteins Proteomics* **1804**, 41–48 (2010).
- D. Demuth, M. Sattig, E. Steinrücken, M. Weigler, and M. Vogel, “ ^2H NMR studies on the dynamics of pure and mixed hydrogen-bonded liquids in confinement,” *Z. Phys. Chem.* **232**, 1059–1087 (2018).
- E. Steinrücken, T. Wissel, M. Brodrecht, H. Breitzke, J. Regentin, G. Buntkowsky, and M. Vogel, “ ^2H NMR study on temperature-dependent water dynamics in amino-acid functionalized silica nanopores,” *J. Chem. Phys.* **154**, 114702 (2021).
- B. Malfait, A. Jani, J. B. Mietner, R. Lefort, P. Huber, M. Fröba, and D. Morineau, “Influence of pore surface chemistry on the rotational dynamics of nanoconfined water,” *J. Phys. Chem. C* **125**, 16864–16874 (2021).
- K. Schröck, F. Schröder, M. Heyden, R. A. Fischer, and M. Havenith, “Characterization of interfacial water in MOF-5 $[\text{Zn}_4(\text{O})(\text{BDC})_3]$ —A combined spectroscopic and theoretical study,” *Phys. Chem. Chem. Phys.* **10**, 4732–4739 (2008).
- Z. L. Terranova and F. Paesani, “The effects of framework dynamics on the behavior of water adsorbed in the $[\text{Zn}(\text{I-L})(\text{Cl})]$ and Co-MOF-74 metal-organic frameworks,” *Phys. Chem. Chem. Phys.* **18**, 8196–8204 (2016).
- M. Sattig, S. Reutter, F. Fajara, M. Werner, G. Buntkowsky, and M. Vogel, “NMR studies on the temperature-dependent dynamics of confined water,” *Phys. Chem. Chem. Phys.* **16**, 19229–19240 (2014).
- M. Weigler, M. Brodrecht, G. Buntkowsky, and M. Vogel, “Reorientation of deeply cooled water in mesoporous silica: NMR studies of the pore-size dependence,” *J. Phys. Chem. B* **123**, 2123–2134 (2019).

- ³³M. Weigler, E. Winter, B. Kresse, M. Brodrecht, G. Buntkowsky, and M. Vogel, "Static field gradient NMR studies of water diffusion in mesoporous silica," *Phys. Chem. Chem. Phys.* **22**, 13989–13998 (2020).
- ³⁴M. Sattig, K. Elamin, M. Reuhl, J. Swenson, and M. Vogel, "Dynamics of DiPGME-water mixtures in mesoporous silica," *J. Phys. Chem. C* **121**, 6796–6806 (2017).
- ³⁵M. Reuhl, M. Weigler, M. Brodrecht, G. Buntkowsky, and M. Vogel, *Molecules* **124**, 20998–21012 (2020).
- ³⁶M. Reuhl, P. Monnard, and M. Vogel, "Confinement effects on glass-forming mixtures: Insights from a combined experimental approach to aqueous ethylene glycol solutions in silica pores," *J. Chem. Phys.* **156**, 084506 (2022).
- ³⁷D. Denysenko, M. Grzywa, M. Tonigold, B. Streppel, I. Krkljus, M. Hirscher, E. Mugnaioli, U. Kolb, J. Hanss, and D. Volkmer, "Elucidating gating effects for hydrogen sorption in MFU-4-type triazolate-based metal-organic frameworks featuring different pore sizes," *Chem. - Eur. J.* **17**, 1837–1848 (2011).
- ³⁸M. Brodrecht, E. Klotz, C. Lederle, H. Breitzke, B. Stühn, M. Vogel, and G. Buntkowsky, "A combined solid-state NMR, dielectric spectroscopy and calorimetric study of water in lowly hydrated MCM-41 samples," *Z. Phys. Chem.* **232**, 1003–1016 (2018).
- ³⁹J. E. Tanner, "Use of the stimulated echo in NMR diffusion studies," *J. Chem. Phys.* **52**, 2523–2526 (1970).
- ⁴⁰B. Geil, "Measurement of translational molecular diffusion using ultra-high magnetic field gradient NMR," *Concepts Magn. Reson.* **10**, 299–321 (1998).
- ⁴¹N. Bloembergen, E. M. Purcell, and R. V. Pound, "Relaxation effects in nuclear magnetic resonance absorption," *Phys. Rev.* **73**, 679 (1948).
- ⁴²F. Noack, "NMR field-cycling spectroscopy: Principles and applications," *Prog. Nucl. Magn. Reson. Spectrosc.* **18**, 171–276 (1986).
- ⁴³F. Fujara, D. Kruk, and A. F. Privalov, "Solid state field-cycling NMR relaxometry: Instrumental improvements and new applications," *Prog. Nucl. Magn. Reson. Spectrosc.* **82**, 39–69 (2014).
- ⁴⁴R. Kimmich and E. Ansaldo, "Field-cycling NMR relaxometry," *Prog. Nucl. Magn. Reson. Spectrosc.* **44**, 257–320 (2004).
- ⁴⁵D. Kruk, A. Herrmann, and E. A. Rössler, "Field-cycling NMR relaxometry of viscous liquids and polymers," *Prog. Nucl. Magn. Reson. Spectrosc.* **63**, 33–64 (2012).
- ⁴⁶M. Becher, A. Lichtinger, R. Minikejew, M. Vogel, and E. A. Rössler, "NMR relaxometry accessing the relaxation spectrum in molecular glass formers," *Int. J. Mol. Sci.* **23**, 5118 (2022).
- ⁴⁷S. Havriliak and S. Negami, "A complex plane analysis of α -dispersions in some polymer systems," *J. Polym. Sci., Part C: Polym. Symp.* **14**, 99–117 (1966).
- ⁴⁸R. Richert, F. Stickel, R. S. Fee, and M. Maroncelli, "Solvation dynamics and the dielectric response in a glass-forming solvent: From picoseconds to seconds," *Chem. Phys. Lett.* **229**, 302–308 (1994).
- ⁴⁹K. Schmidt-Rohr and H. W. Spiess, *Multidimensional Solid-State NMR and Polymers* (Academic Press, 1994).
- ⁵⁰R. Böhmer, G. Diezemann, G. Hinze, and E. Rössler, "Dynamics of supercooled liquids and glassy solids," *Prog. Nucl. Magn. Reson. Spectrosc.* **39**, 191–267 (2001).
- ⁵¹D. Schaefer, J. Leisen, and H. W. Spiess, "Experimental aspects of multi-dimensional exchange solid-state NMR," *J. Magn. Reson., Ser. A* **115**, 60–79 (1995).
- ⁵²B. Kresse, M. Becher, A. F. Privalov, M. Hofmann, E. A. Rössler, M. Vogel, and F. Fujara, "¹H NMR at Larmor frequencies down to 3 Hz by means of field-cycling techniques," *J. Magn. Reson.* **277**, 79–85 (2017).
- ⁵³S. A. Lusceac and M. Vogel, "²H NMR study of the water dynamics in hydrated myoglobin," *J. Phys. Chem. B* **114**, 10209–10216 (2010).
- ⁵⁴C. R. Herbers, D. Sauer, and M. Vogel, "²H NMR studies of glycerol dynamics in protein matrices," *J. Chem. Phys.* **136**, 124511 (2012).
- ⁵⁵M. Reuhl, P. Monnard, and M. Vogel, "Effects of partial crystallization on the glassy slowdown of aqueous ethylene glycol solutions," *J. Chem. Phys.* **155**, 224501 (2021).
- ⁵⁶M. Vogel and E. Rössler, "On the nature of slow β -process in simple glass formers: A ²H NMR study," *J. Phys. Chem. B* **104**, 4285–4287 (2000).
- ⁵⁷B. Geil, F. Fujara, and H. Sillescu, "²H NMR time domain analysis of ultraslow reorientations in supercooled liquids," *J. Magn. Reson.* **130**, 18–26 (1998).
- ⁵⁸R. Böhmer and G. Hinze, "Reorientations in supercooled glycerol studied by two-dimensional time-domain deuteron nuclear magnetic resonance spectroscopy," *J. Chem. Phys.* **109**, 241–248 (1998).
- ⁵⁹G. Hinze, "Geometry and time scale of the rotational dynamics in supercooled toluene," *Phys. Rev. E* **57**, 2010–2018 (1998).
- ⁶⁰M. Vogel and E. Rössler, "Effects of various types of molecular dynamics on 1D and 2D ²H NMR studied by random walk simulations," *J. Magn. Reson.* **147**, 43–58 (2000).
- ⁶¹M. Vogel and E. Rössler, "Slow β process in simple organic glass formers studied by one- and two-dimensional ²H nuclear magnetic resonance. I," *J. Chem. Phys.* **114**, 5802–5815 (2001).
- ⁶²M. Vogel and E. Rössler, "Slow β process in simple organic glass formers studied by one- and two-dimensional ²H nuclear magnetic resonance. II. Discussion of motional models," *J. Chem. Phys.* **115**, 10883–10891 (2001).
- ⁶³Z. Wang, P. Le, K. Ito, J. B. Leão, M. Tyagi, and S.-H. Chen, "Dynamic crossover in deeply cooled water confined in MCM-41 at 4 kbar and its relation to the liquid-liquid transition hypothesis," *J. Chem. Phys.* **143**, 114508 (2015).
- ⁶⁴S. Lemke, P. H. Handle, L. J. Plaga, J. N. Stern, M. Seidl, V. Fuentes-Landete, K. Amann-Winkel, K. W. Köster, C. Gainaru, T. Loerting, and R. Böhmer, "Relaxation dynamics and transformation kinetics of deeply supercooled water: Temperature, pressure, doping, and proton/deuteron isotope effects," *J. Chem. Phys.* **147**, 034506 (2017).
- ⁶⁵C. Gainaru, A. L. Agapov, V. Fuentes-Landete, K. Amann-Winkel, H. Nelson, K. W. Köster, A. I. Kolesnikov, V. N. Novikov, R. Richert, R. Böhmer, T. Loerting, and A. P. Sokolov, "Anomalous large isotope effect in the glass transition of water," *Proc. Natl. Acad. Sci. U. S. A.* **111**, 17402–17407 (2014).
- ⁶⁶Y. Beilinson, V. Schiller, J. Regentin, J. H. Melillo, A. Greenbaum, T. Antropova, S. Cervený, M. Vogel, and Y. Feldman, "The nature of the low-temperature crossover of water in hard confinement," *J. Phys. Chem. B* **127**, 5128–5140 (2023).
- ⁶⁷W. Schnauss, F. Fujara, and H. Sillescu, "The molecular dynamics around the glass transition and in the glassy state of molecular organic systems: A ²H-nuclear magnetic resonance (NMR) study," *J. Chem. Phys.* **97**, 1378 (1992).
- ⁶⁸M. Alcoultabi and G. B. McKenna, "Effects of confinement on material behavior at the nanometre size scale," *J. Phys.: Condens. Matter* **17**, R461–R524 (2005).
- ⁶⁹R. Richert, "Dynamics of nanoconfined supercooled liquids," *Annu. Rev. Phys. Chem.* **62**, 65–84 (2011).
- ⁷⁰M. Arndt, R. Stannarius, H. Groothues, E. Hempel, and F. Kremer, "Length scale of cooperativity in the dynamic glass transition," *Phys. Rev. Lett.* **79**, 2077–2080 (1997).
- ⁷¹G. Barut, P. Pissis, R. Pelster, and G. Nimtz, "Glass transition in liquids: Two vs three-dimensional confinement," *Phys. Rev. Lett.* **80**, 3543–3546 (1998).
- ⁷²P. Scheidler, W. Kob, and K. Binder, "The relaxation dynamics of a supercooled liquid confined by rough walls," *J. Phys. Chem. B* **108**, 6673–6686 (2004).
- ⁷³W. Kob, S. Roldán-Vargas, and L. Berthier, *Nat. Phys.* **8**, 164–167 (2012).
- ⁷⁴R. Horstmann, L. Hecht, S. Kloth, and M. Vogel, "Structural and dynamical properties of liquids in confinements: A review of molecular dynamics simulation studies," *Langmuir* **38**, 6506–6522 (2022).